CHEMISTRY OF MATERIALS

Article

pubs.acs.org/cm

Atomic Layer Deposition of Ruthenium and Ruthenium Oxide Using a Zero-Oxidation State Precursor

Dustin Z. Austin,[†] Melanie A. Jenkins,[†] Derryl Allman,[‡] Sallie Hose,[‡] David Price,[‡] Charles L. Dezelah,[§] and John F. Conley, Jr.*[,†]

[†]School of Electrical Engineering and Computer Science, Oregon State University, Corvallis, Oregon 97330, United States

[‡]Technology Development, ON Semiconductor, Gresham, Oregon 97030, United States

[§]EMD Performance Materials, Haverhill, Massachusetts 01832, United States

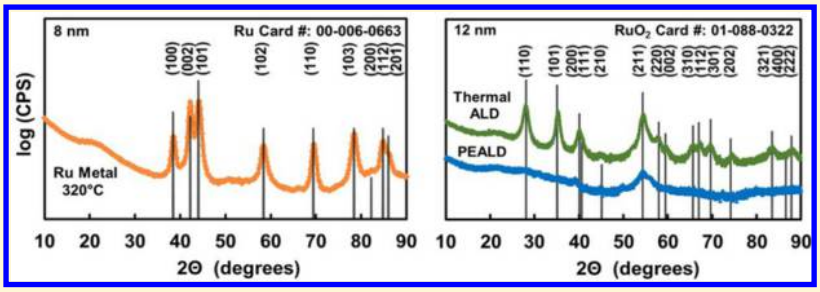

ABSTRACT: Atomic layer deposition (ALD) processes are reported for ruthenium (Ru) and ruthenium oxide (RuO_2) using a zero-oxidation state liquid precursor, η^4-2,3-dimethylbutadiene ruthenium tricarbonyl [$Ru(DMBD)(CO)_3$]. Both ALD Ru and RuO_2 films were deposited using alternating N_2 -purge-separated pulses of $Ru(DMBD)(CO)_3$ and O_2. ALD Ru metal films were deposited via short (2 s) pulses of O_2. Ru films have an ALD temperature window from 290 to 320 °C with a GPC of 0.067 nm/cycle and a negligible nucleation delay on SiO_2. Ru films show a strong hexagonal crystal structure with low resistivity of approximately 14 $\mu\Omega$ cm at 320 °C. RuO_2 films were deposited using longer (20 s) pulses of either molecular O_2 or O_2 plasma. RuO_2 films deposited via thermal ALD using molecular O_2 have a temperature window from 220 to 240 °C with a GPC and nucleation delay on SiO_2 of 0.065 nm/cycle and 35 cycles, respectively. Thermal ALD RuO_2 films show a distinct rutile phase microstructure with a resistivity of approximately 62 $\mu\Omega$ cm. In comparison to thermal ALD, the PEALD RuO_x films show a lower growth rate and higher nucleation delay of 0.029 nm/cycle and 76 cycles, respectively. PEALD RuO_x films also exhibit less distinct crystallinity and a higher resistivity of 377 $\mu\Omega$ cm.

1. INTRODUCTION

Atomic layer deposition (ALD) is a technique that has received a considerable and growing amount of attention because of its ability to provide uniform and conformal layers of solid materials, often with subnanometer control over thickness. In particular, ALD has found important applications in the microelectronics industry, where dielectrics are now well established and conductive films, including ruthenium-containing layers, have become the focal point of much research. Ruthenium metal has a low bulk resistivity (7.1 $\mu\Omega$ cm), a high work function (4.7 eV), and a low solid solubility with strong adhesion to Cu, making Ru an attractive barrier metal or seed layer for Cu electroplating.[1] Ruthenium oxide (RuO_2) also has a low resistivity (46 $\mu\Omega$ cm), an even higher work function (5.1 eV), and a good chemical stability, making RuO_2 of interest as an electrode for CMOS transistors and high-κ metal−insulator−metal capacitors.[2−4] Its relatively high chemical stability makes RuO_2 less likely to form an interfacial layer during dielectric deposition than commonly used bottom electrodes such as TaN and TiN. Unwanted interfacial layers can comprise a substantial percentage of the dielectric thickness and reduce the maximal achievable capacitance.[5] In addition, prior work with RuO_2 has demonstrated that it may be used to template the high-κ rutile phase of TiO_2 at reduced deposition temperatures.[2−4] Because of its inherent advantages relative to traditional film growth methods, ALD processes for Ru and RuO_2 are strongly desired for coating the high-aspect ratio structures encountered in the back end of line of ultra large-scale integration (ULSI) process flows.

A key limiting factor in the implementation of ALD for emerging applications is the development of new process chemistry that affords optimal film growth characteristics. For example, $Ru(EtCp)_2$, currently the most widely reported Ru ALD precursor and commonly used in CVD processes, lacks a clear thermal ALD deposition window and shows very long nucleation delays on SiO_2 and TaN surfaces for both Ru and RuO_2 deposition.[6−15] Although the incorporation of NH_3 plasma has been shown to improve the nucleation and growth problems, the process is not ideal because of the toxicity, added expense, and intrinsic aspect ratio limitations of plasma-based

Received: October 5, 2016
Revised: January 13, 2017
Published: January 17, 2017

DOI: 10.1021/acs.chemmater.6b04251
Chem. Mater. 2017, 29, 1107−1115

processes.[12,13] As Ru and RuO_2 films in ULSI applications are generally only a few to tens of nanometers thick, nucleation delay is a critical growth parameter. When a large number of cycles is required to obtain a continuous film, it not only can dramatically increase the deposition time, decreasing throughput and increasing cost considerably in manufacturing, but also can result in rougher interfaces because of island-like nucleation. Other Ru precursors with non-zero oxidation states also typically exhibit long nucleation delays for Ru and RuO_2 when grown by thermal ALD.[6−9,16−27] More recent work has shown Ru(0) complexes can significantly reduce nucleation delays for O_2-based thermal ALD processes.[28−34] Most Ru(0) ALD precursors contain an η^6-arene ligand, while most higher-oxidation state precursors contain one or more cyclopentadienyl ligands, or a substituted variant thereof.[35] Herein, we report a previously unexplored Ru(0) precursor, η^4-2,3-dimethylbutadiene ruthenium tricarbonyl [$Ru(DMBD)(CO)_3$], which is unusual in that it contains neither arene nor cyclopentadienyl ligands. Only a small number of ALD studies have used zero-oxidation state Ru precursors containing a butadiene type ligand.[28−34,36,37] Alkene ligands, including butadiene derivatives, may help stabilize low-oxidation state metal complexes because of their ability to engage in π backbonding. However, in all but two cases, the previously reported butadiene-bearing Ru(0) precursors also contain an η^6-arene ligand.[36,37] $Ru(DMBD)(CO)_3$ also possesses carbonyl ligands, which are known to readily undergo dissociation from metal centers.[38] We propose that the lability of carbonyl together with the stabilizing influence of DMBD allows the precursor to facilitate rapid nucleation on a surface, while also delivering a robust process capable of performing ALD at temperatures in excess of 300 °C.

In this work, we develop and characterize a thermal ALD process for Ru metal as well as both thermal ALD and PEALD processes for RuO_2 using $Ru(DMBD)(CO)_3$ and oxygen.

2. EXPERIMENTAL PROCEDURES

$Ru(DMBD)(CO)_3$ was obtained from EMD Performance Materials and was used for deposition experiments as received without further purification. $Ru(DMBD)(CO)_3$ can be synthesized on a laboratory scale from $Ru_3(CO)_8$ and DMBD using a method reported previously for Ru diene complexes.[39] Thermogravimetric analysis (TGA) of $Ru(DMBD)(CO)_3$ was performed in a TA Instruments model Q50 system with a temperature ramp rate of 10 °C/min under a nitrogen ambient at atmospheric pressure. Vapor pressure was determined from isothermal TGA measurements using a method described previously.[40]

ALD of Ru and RuO_2 was performed in a Picosun SUNALE R-200 reactor at 6 Torr using alternating N_2-purge-separated pulses of $Ru(DMBD)(CO)_3$ and either molecular O_2 or oxygen plasma on Si substrates with 100 nm of thermally grown SiO_2. All depositions followed a reactor conditioning process that coated the chamber with ∼50 nm of either Ru or RuO_2, depending on the intended film. Flow rates in all source lines were held at 150 sccm, except for the O_2 line, which used 180 sccm of O_2 with either 150 or 50 sccm N_2 carrier gas for ruthenium metal or ruthenium oxide, respectively. As reported previously for Ru processes, the O_2 partial pressure is important for determining the composition of the deposited film.[7,8]

$Ru(DMBD)(CO)_3$, shown in the inset of Figure 1a, is a zero-oxidation state precursor that is liquid at room temperature. A vapor pressure between 1 and 2 Torr is achieved over a wide temperature range of 35−60 °C, shown in Figure 1a. In Figure 1b, the TGA curve and the associated derivative reveal a single weight loss event from ∼80 to 130 °C, after which <1% of the original precursor mass remains. This observation is consistent with complete clean volatilization without nonvolatile residues remaining. TGA alone, however, cannot rule out decomposition products that may evaporate concurrently with the precursor. Although a decomposition event concurrent with volatilization could result in a derivative curve with multiple peaks, this was not observed for this compound. On the basis of the vapor pressure and TGA, a precursor temperature of 45 °C was chosen to give a sufficient dose while limiting aging of the $Ru(DMBD)(CO)_3$ due to temperature stressing.

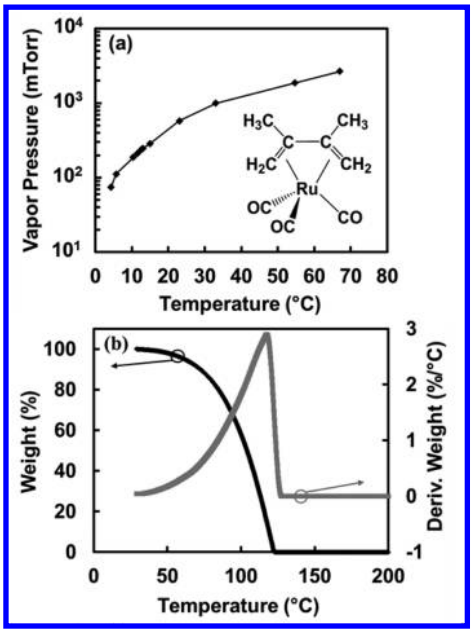

Figure 1. (a) Vapor pressure vs temperature for $Ru(DMBD)(CO)_3$ with the inset showing molecular structure. (b) TGA % weight remaining vs temperature and derivative for $Ru(DMBD)(CO)_3$.

Film morphology, density, thickness, and interfacial roughness were investigated via X-ray reflectivity (XRR) and grazing incidence X-ray diffraction (GIXRD) using a Rigaku Ultima IV instrument with Cu Kα radiation (λ = 1.5406 Å). RuO_2 film thickness was measured using a J. A. Woollam M2000 spectroscopic ellipsometer (SE) in the range of 400−1000 nm. Surface roughness was measured via atomic force microscopy (AFM) using an Asylum Research MFP-3D instrument in tapping mode with a 1 Hz scan rate. Resistivity was measured via a four-point probe. Compositional analysis was performed using a combination of X-ray photoelectron spectroscopy (XPS) and Auger electron spectroscopy (AES) via a PHI VersaProbe II with excitation from monochromatic Al Kα X-ray radiation ($h\nu$ = 1486.6 eV), with a 15 keV X-ray beam voltage, and sputtered with 2 keV argon ions.

3. RESULTS

3.1. ALD Ru. The growth of Ru films was studied using a thermal ALD process in which $Ru(DMBD)(CO)_3$ and O_2 were alternately pulsed into the deposition chamber. Shown in Figure 2 is a plot of Ru film thickness, measured via XRR, versus deposition temperature. Using 2.0 s O_2 pulses and 1.5 s $Ru(DMBD)(CO)_3$ pulses separated by 30 s N_2 purges, an ALD window (defined here as a relatively constant film thickness) was found between 290 and 320 °C. The film deposited at 320 °C has a density of 12.2 g/cm^3, which is just below the bulk value of Ru (12.37 g/cm^3).[41] Also shown in Figure 2, the resistivity slightly decreased with an increase in deposition temperature, ranging from ∼18 $\mu\Omega$ cm at 290 °C to ∼14 $\mu\Omega$ cm at 320 °C.

The effect of $Ru(DMBD)(CO)_3$ pulse time on film thickness, while all other variables are held constant, is shown in Figure 3a. Self-limited saturating growth was observed with Ru pulse times of >1.5 s. Shorter pulse times resulted in either less growth (0.6 and 0.9 s) or more growth (1.2 s). With

DOI: 10.1021/acs.chemmater.6b04251
Chem. Mater. 2017, 29, 1107−1115

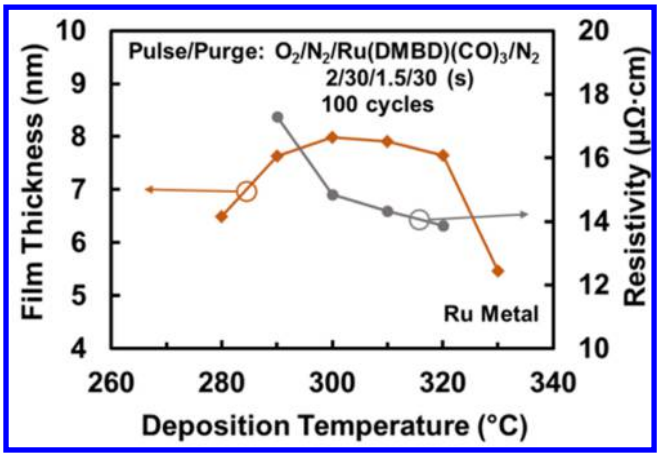

Figure 2. Film thickness and resistivity vs deposition temperature for ALD Ru metal.

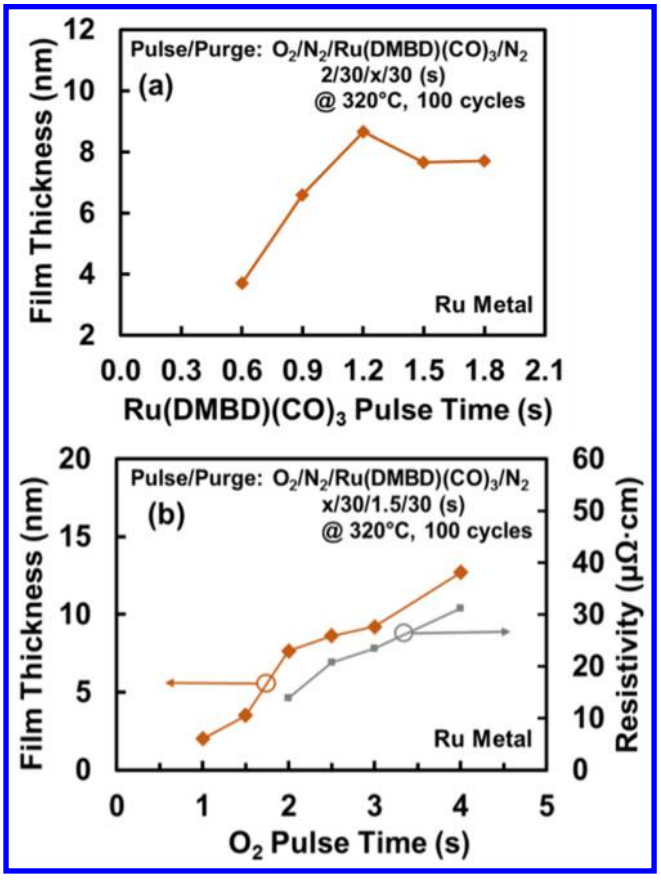

Figure 3. Film thickness vs (a) $Ru(DMBD)(CO)_3$ pulse time and (b) O_2 pulse time for ALD Ru metal.

respect to O_2 pulse time, shown in Figure 3b, the deposition rate showed a soft saturation between 2 and 3 s with a large increase observed when longer O_2 exposures were used. As discussed below, this is suggestive of an increase in the rate of uptake of oxygen into films when using O_2 doses beyond the amount needed for the reaction to form metallic Ru. To rule out growth due to possible precursor decomposition, a control run with 200 ALD cycles of $Ru(DMBD)(CO)_3$ without the oxygen co-reactant (1.2, 30, 0, and 30 s for Ru, N_2, O_2, and N_2, respectively) at 300 °C resulted in no measurable deposition on the SiO_2/Si substrate.

Shown in Figure 4 is a plot of Ru film thickness as a function of the number of deposition cycles. ALD Ru metal was found to

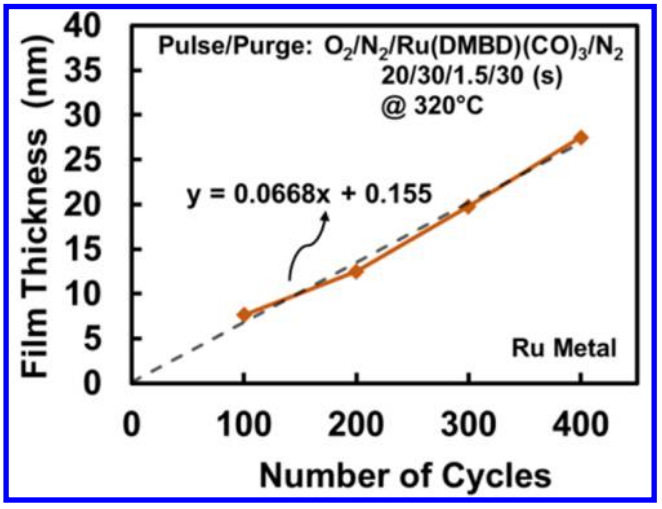

Figure 4. Film thickness vs the number of ALD cycles for ALD Ru metal.

have a linear growth per cycle (GPC) of 0.067 nm/cycle at 320 °C with a negligible nucleation delay. Nucleation delay was estimated by extrapolating the linear fit to the *x*-axis. Because the *x*-intercept of the best-fit line crossed very near the origin, it can be surmised that the initial stages of growth proceeded at a rate having very little deviation from that observed with a larger number of deposition cycles, a good indication that a significant nucleation delay did not occur.

Compositional analysis of a 20 nm thick Ru film deposited at 320 °C was performed using a combination of XPS and AES and is shown in Figure 5. The film was sputtered using 2 keV argon ions for 30 s to the approximate midpoint depth of the film. Peaks for the Ru $3d_{5/2}$ and Ru $3d_{3/2}$ ionizations were observed at 280.1 and 284.3 eV, respectively, and are consistent with metallic Ru but are also similar to the reported values for RuO_2.[42] The oxygen content was below the detection limits of the instrument (<0.1%). Because of the overlap of the C 1s

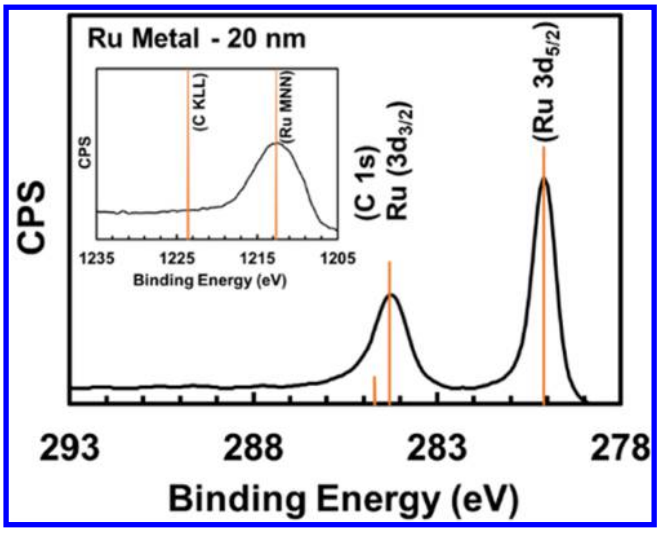

Figure 5. High-resolution XPS spectrum of Ru $3d_{5/2}$ and Ru $3d_{3/2}$ ionizations for ALD Ru metal film with an inset of high-resolution AES regions for C KLL and Ru MNN.

DOI: 10.1021/acs.chemmater.6b04251
Chem. Mater. 2017, 29, 1107−1115

region with the Ru $3d_{3/2}$ region, carbon could not be easily quantified by XPS. Inspection of the AES spectrum in the region of the C KLL transition revealed that carbon was below the detection limit.

GIXRD confirmed a polycrystalline hexagonal microstructure with no preferred orientation for an 8 nm thick Ru film deposited at 320 °C (Figure 6). An average crystal size of ~7.6 nm was estimated using the Scherrer formula. In Figure 7, AFM measurement of the same film showed 0.6 nm RMS surface roughness.

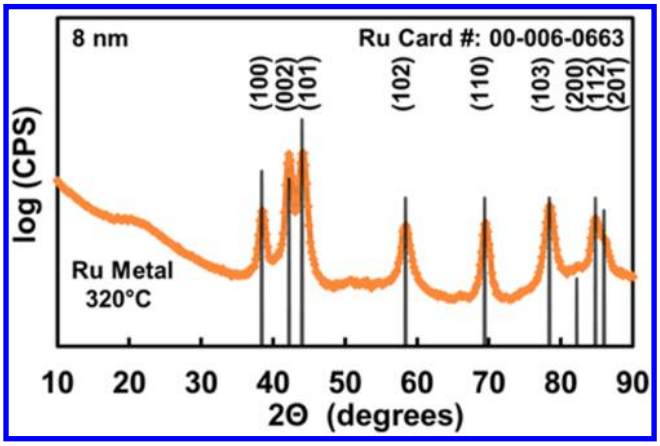

Figure 6. GIXRD plot of log intensity vs 2θ for an 8 nm thick ALD Ru metal film deposited at 320 °C with a reference card pattern overlay.

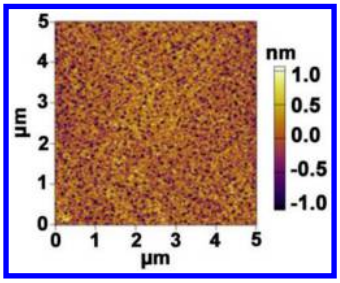

Figure 7. AFM surface roughness measurements of an 8 nm thick ALD Ru metal film deposited at 320 °C.

3.2. ALD RuO_2. Using the same $Ru(DMBD)(CO)_3$ precursor, RuO_2 was investigated via (a) thermal ALD with molecular O_2 and (b) PEALD using plasma-generated oxygen radicals as the co-reactant. Plots of film thickness versus deposition temperature are shown in Figure 8 for both ALD processes. Clear ALD temperature windows were evident for both thermal and plasma processes. Both RuO_2 process windows required lower temperatures and much longer (20 s) oxidant exposures, as compared to the Ru process (2 s O_2 exposures) discussed previously. For thermal ALD, a 20 °C wide RuO_2 window with a nearly constant film thickness was observed between 220 and 240 °C, with the best nonuniformity (~2.8% across a 6 in. wafer) observed at a deposition temperature of 240 °C. In comparison, the PEALD RuO_2 process exhibited an ALD window with a range of 30 °C, shifted to slightly lower temperatures (200–230 °C). PEALD films showed a degraded nonuniformity of 4.5% at 230 °C. For both processes, the deposition rate dropped off at temperatures below the ALD window and increased at temperatures above the ALD window.

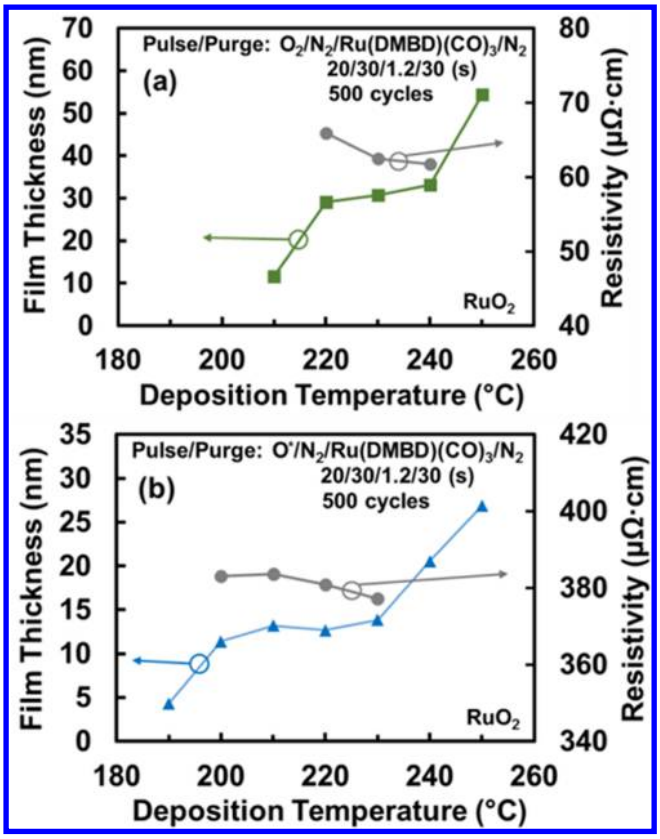

Figure 8. Film thickness and resistivity vs deposition temperature for (a) thermal ALD and (b) PEALD of RuO_2.

Also included in Figure 8 are plots of resistivity versus deposition temperature for both the (a) ALD and (b) PEALD processes. Within the respective ALD windows, resistivity for both processes decreased slightly with increasing temperature. The thermal ALD RuO_2 films had a resistivity as low as ~62 $\mu\Omega$ cm, while that of the PEALD films was much higher (~377 $\mu\Omega$ cm).

$Ru(DMBD)(CO)_3$ pulse saturation curves for both thermal and PEALD processes using 20 s O_2 pulses are shown in Figure 9a. Saturation occurred at roughly the same precursor pulse length for both processes, at around 0.8 s for the thermal O_2 process and approximately 1.0 s for the PEALD process. The $Ru(DMBD)(CO)_3$ saturation behavior was not substantially different at 20 or 30 s O_2 pulse lengths. Experiments were also performed to examine the O_2 pulse saturation, as shown in Figure 9b for the thermal O_2 process. Saturation of the O_2 pulse time occurred at approximately 20 s. Films deposited with a shorter 5 s pulse time exhibit reduced resistivity (~40 $\mu\Omega$ cm), indicating a more metallic character.

The deposition rates for the two processes were found to be significantly different. Shown in Figure 10 is a plot of RuO_2 film thickness versus the number of ALD cycles for both ALD and PEALD. Thermal ALD (0.065 nm/cycle) had more than double the GPC of PEALD (0.029 nm/cycle). The nucleation delay, estimated by extrapolating a linear fit back to the x-axis, was also better for the thermal ALD process, being approximately 35 cycles for thermal ALD and roughly 76 cycles for PEALD.

The analysis of a 20 nm thick RuO_2 film deposited at 240 °C was performed using XPS and AES, shown in Figure 11. The film was sputtered using 2 keV argon ions for 30 s to the

DOI: 10.1021/acs.chemmater.6b04251
Chem. Mater. 2017, 29, 1107–1115

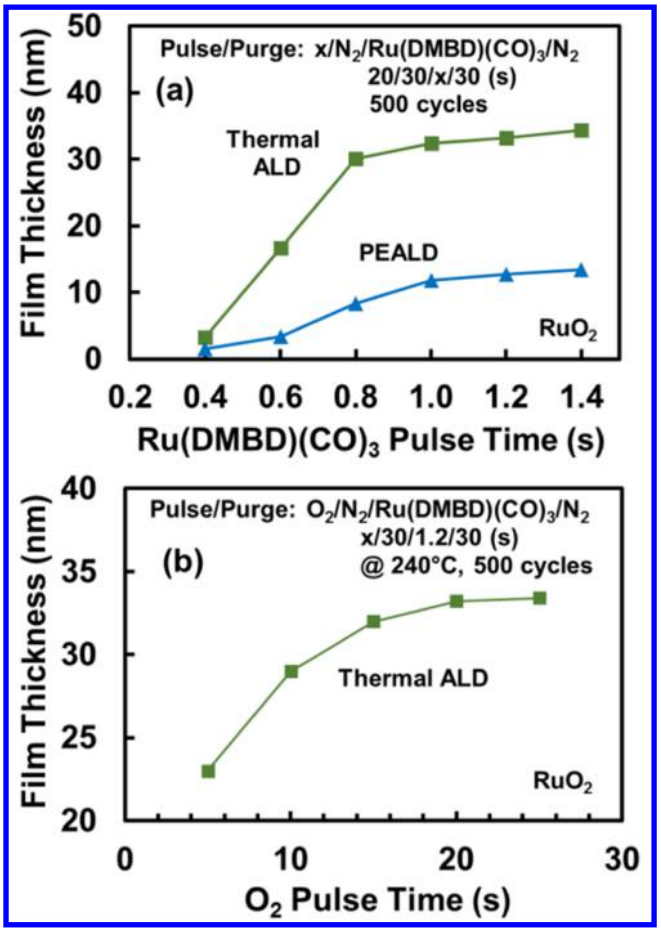

Figure 9. (a) $Ru(DMBD)(CO)_3$ pulse time saturation curve for thermal ALD (green squares) and PEALD (blue triangles) of RuO_2 and (b) O_2 pulse time saturation curve for thermal ALD of RuO_2.

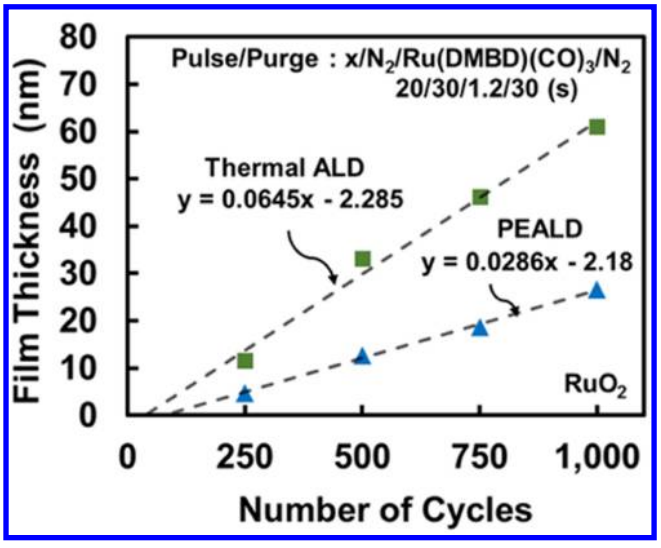

Figure 10. Film thickness vs the number of ALD cycles for thermal ALD (green squares) and PEALD (blue triangles) of RuO_2.

approximate the midpoint depth of the film. Peaks for the Ru $3d_{5/2}$ and Ru $3d_{3/2}$ ionizations were observed at 280.3 and 284.5 eV, respectively, which are consistent with RuO_2 and distinct from other oxides of Ru.[42] The O 1s peak was detected at 529.7 eV. The film composition was measured at 34.7% Ru and 65.2% O, which indicates slightly Ru-rich films. Preferential

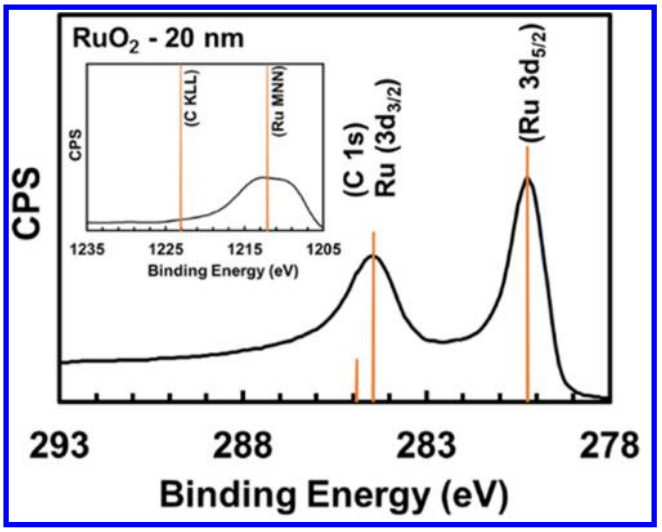

Figure 11. High-resolution XPS spectrum of Ru $3d_{5/2}$ and Ru $3d_{3/2}$ ionizations of an ALD RuO_2 film with an inset of the high-resolution AES region for C KLL and Ru MNN.

sputtering of oxygen is the likely cause of deviation from the expected RuO_2 stoichiometry. Because of the overlap of the C 1s region with the Ru $3d_{3/2}$ region, carbon could not be easily quantified by XPS. Inspection of the AES spectrum in the region of the C KLL transition revealed that carbon was below the detection limit.

Shown in Figure 12 are GIXRD scans of intensity versus 2θ for ~12 nm thick RuO_2 films deposited using either thermal

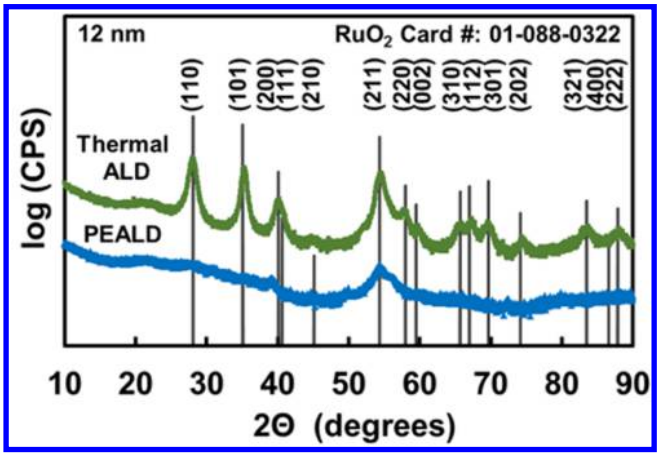

Figure 12. GIXRD plots of log intensity vs 2θ for 12 nm thick RuO_2 films via thermal ALD (green squares) and PEALD (blue triangles) deposited at 240 and 230 °C, respectively.

ALD at 240 °C or PEALD at 230 °C. The crystal structure of the films showed significant differences. The thermal ALD RuO_2 film exhibited a strong set of peaks corresponding to the rutile (tetragonal) phase with an average Scherrer estimated grain size of ~3.6 nm, whereas the PEALD RuO_2 showed only one minor peak, the 54° (211) peak of the rutile phase. In Figure 13, AFM images of the same films showed that the thermal ALD film has a surface RMS roughness (0.6 nm) slightly higher than that of the PEALD film (0.4 nm). XRR measurements of the same films also showed the ALD RuO_2 to be at 6.77 g/cm^3, just below bulk rutile (tetragonal) RuO_2 (6.97 g/cm^3), while the PEALD RuO_2 was at 7.91 g/cm^3.

DOI: 10.1021/acs.chemmater.6b04251
Chem. Mater. 2017, 29, 1107−1115

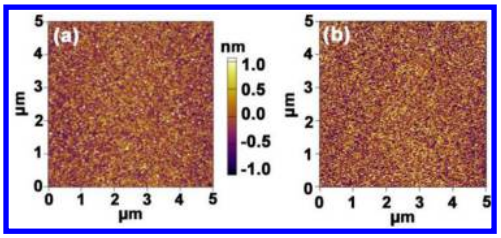

Figure 13. AFM images of 12 nm thick (a) thermal ALD and (b) PEALD RuO_2 films deposited at 240 and 230 °C, respectively.

4. DISCUSSION

4.1. Ru Process. The Ru process pulse saturation behavior in Figure 3a exhibited a higher deposition rate at a 1.2 s $Ru(DMBD)(CO)_3$ pulse length, prior to eventual saturation at 1.5 s. This sort of behavior is sometimes an indication of self-etching of the deposited film.[43] However, the increased deposition rate was accompanied by an increased resistivity (~30 $\mu\Omega$ cm at 1.2 s). Depending on the surface morphology, oxygen can penetrate beneath Ru film surfaces at temperatures as low as 250 °C.[44] As described by Aaltonen et al., this subsurface oxygen that is incorporated during the O_2 pulse (and remains through the N_2 purge) is mobile and can participate in oxidative decomposition of ligands during the subsequent $Ru(DMBD)(CO)_3$ pulse.[45] If this subsurface O_2 is completely consumed during the Ru precursor pulse, Ru may be deposited. If it is not completely consumed, then RuO_2 (thermodynamically favored at the deposition temperature[46]) may result. The increased deposition rate and resistivity at 1.2 s Ru precursor pulse lengths thus point toward incorporation of oxygen into the film to form substoichiometric RuO_x, likely due to incomplete consumption of the subsurface oxygen during the Ru precursor pulse.[10,17,45] This is consistent with the O_2 pulse time dependence (Figure 3b), which exhibited an increasing film thickness accompanied by an increasing resistivity. For fixed 1.5 s Ru precursor pulses, the continued increase in deposition rate at 4 s of O_2 pulse time could have been due to a larger O_2 reservoir in the subsurface available for reaction during the Ru precursor pulse, again resulting in RuO_x.

Table 1 contains a summary of thermal ALD Ru processes to date that have used O_2 as a co-reactant, including the precursor, nucleation delay, GPC, ALD temperature window, and film resistivity. In this work, Ru films were deposited using $Ru(DMBD)(CO)_3$ and O_2. A saturating growth rate of 0.067 nm/cycle with a negligible nucleation delay on SiO_2 was observed within an ALD temperature window of 290−320 °C. The GPC and ALD windows were comparable to or higher than the other Ru(0) ALD precursors listed in Table 1. The negligible nucleation delay found for $Ru(DMBD)(CO)_3$ was much less than the ~210 cycles observed for $Ru(EtCp)_2$ when it was deposited without NH_3 plasma and also shorter than the long nucleation delays reported for other higher-oxidation state Ru precursors.[6−9,16−27] The negligible nucleation delay for $Ru(DMBD)(CO)_3$ is as good as or better than those of previously reported Ru(0) precursors.[28−33] The generally short nucleation delays observed using Ru(0) precursors versus higher-oxidation state precursors in Table 1 are possibly due to a lower thermodynamic activation energy barrier.[28,33] A smaller barrier could be the result of the lack of reduction needed for the metal to achieve the Ru(0) form present in the final thin film material. It could also be due to the exclusively neutral ligands present on Ru(0) complexes, which are more susceptible to dissociation than the anionic ligands that are found on higher-oxidation state Ru precursors.

The hexagonal Ru microstructure exhibits no RuO_2-associated peaks and an average crystal size of roughly 7.6 nm for an 8 nm thick film (Figure 5). Crystallite size has been shown to increase with film thickness because of a columnar microstructure that grows vertically.[23,37,47] The Ru film resistivity at 320 °C was approximately 14 $\mu\Omega$ cm, roughly double the bulk Ru resistivity, but lower than or comparable to values from other reports of thin film ALD Ru, as indicated in Table 1. The low resistivity is consistent with phase purity and low carbon content (found to be below the detection limit of AES analysis). Finally, the RMS roughness of 0.6 nm for an 8 nm thick film (Figure 7) was also comparable to values from other reports.[28]

4.2. RuO_2 Process. Table 2 contains a summary of ALD RuO_2 processes to date, including the precursor, nucleation delay, GPC, ALD temperature window, and film resistivity. Using long (20 s) oxygen pulses and lower temperatures, RuO_2 films were deposited by both thermal and PEALD using $Ru(DMBD)(CO)_3$ and either O_2 or O_2 plasma, respectively. The temperature window for thermal ALD RuO_2 (220−240 °C) is slightly higher than that of PEALD RuO_2 (200−230 °C). Thermal RuO_2 exhibits a GPC higher than and a nucleation delay on SiO_2 substrates shorter than those of PEALD RuO_2, with 0.065 and 0.029 nm/cycle and 35 and 76 cycles,

Table 1. Comparison of Ruthenium Precursors for Thermal ALD Ru Processes Using O_2 as a Co-Reactant

precursor	metal oxidation state	nucleation (no. of cycles)	growth rate (nm/cycle)	ALD window (°C)	resistivity ($\mu\Omega$ cm)	refs
$Ru(thd)_3$	+3	~250	0.036	325−450	15−20	17
$Ru(EtCp)_2$	+2	~210[13]	0.049[13]	uncertain[7]	15[13]	6−9, 12, 13
$Ru(Cp)_2$	+2	~250[16]	0.045[16]	325−375[16]	13[16]	16, 18
ECPR	+2	~25[20]	0.09[20]	uncertain[20]	22−26[20]	19, 20
DMPR	+2	~60	0.022	250−320	18−24	21
Cyprus	+2	~20	0.05	250−310	20	22
$Ru(DMPD)_2$	+2	~40[23]	0.012[23]	185−210[23]	17[24]	23, 24
$Ru(Cp)(CO)_2Et$	+2	~85[25]	0.1[25]	300−325[26]	16[25]	25, 26
$(HD)^iPrMePhRu$	0	3	0.076	270−350	29−36	28
IMBCHDRu	0	~10[29]	0.089[29]	225−270[29]	30−40[29]	29, 30
EBCHDRu	0	3	0.1	200−275	18	31
EBECHDRu	0	3	0.042	175−275	20	32
EBBDRu	0	15	0.056	not available	26	33
$Ru(DMBD)(CO)_3$	0	~0	0.067	290−320	14	this work

DOI: 10.1021/acs.chemmater.6b04251
Chem. Mater. 2017, 29, 1107−1115

Table 2. Comparison of Ruthenium Precursors for RuO_2

precursor	metal oxidation state	nucleation (no. of cycles)	growth rate (nm/cycle)	ALD window (°C)	resistivity ($\mu\Omega$ cm)	refs
$Ru(EtCp)_2$	+2	~700[6]	0.175[9]	not available	70[9]	6, 8, 9
Ru(Cp)2	+2	not available	0.32	not available	270	18
$Ru(DMPD)_2$	+2	~125	0.023	not available	not available	23
$(HD)^iPrMePhRu$	0	−50	0.15	180−200	275	28
EBCHDRu	0	2	0.186	not available	118	34
EBBDRu	0	6	0.09	not available	~140	33
$Ru(DMBD)(CO)_3$	0	35	0.065	220−240	62	this work

respectively. Many of the previous RuO_2 processes listed in Table 2 report growth rates that are greater than that typically observed for ALD (GPC $\lesssim$ 0.15 nm/cycle). As such, it is likely that they contain a CVD component. The GPC reported here is more typical of the submonolayer per cycle growth expected for a well-behaved ALD process. RuO_2 films grown in this work by thermal ALD show a distinct rutile phase microstructure, a resistivity of ~62 $\mu\Omega$ cm, and a close to bulk density (6.97 g/cm^3), whereas the PEALD RuO_2 films have less distinct crystallinity, much higher resistivity (~377 $\mu\Omega$ cm), and increased density (7.91 g/cm^3). This resistivity for thermal ALD RuO_2 is approximately half of what is reported for many of the other available RuO_2 capable precursors, listed in Table 2. Considering morphology, thermal ALD RuO_2 is preferred for templating the high-k rutile phase of TiO_2. Unlike other Ru(0) precursors, the thermal ALD RuO_2 grown using $Ru(DMBD)(CO)_3$ has no Ru metal peaks, which may improve its ability to template TiO_2. The reduced GPC and increased nucleation delay for the PEALD process are likely due to the use of oxygen plasma, which is known to etch RuO_2.[48] Likewise, the lack of crystal structure in the PEALD films may be also be due to the interruption of grain growth by oxygen plasma etching during deposition. This lack of crystal structure in turn likely accounts for the much higher resistivity and reduced surface roughness.

4.3. Comparing Ru and RuO_2 Processes. In this work, both Ru and RuO_2 were deposited using the same $Ru(DMBD)(CO)_3$ precursor and O_2 reactant. To improve our understanding of why this is possible, the GPC and resistivity versus temperature data from Figures 2 and 8 are combined in Figure 14. Whereas the window for the Ru process is from 290 to 320 °C, the window for the RuO_2 process is from 220 to 240 °C. The lower-temperature ALD window for RuO_2 as compared to Ru metal is consistent with the findings of Jung et al. for (1,5-hexadiene)(1-isopropyl-4-methylbenzene)-Ru(0).[28] It has been reported previously that the formation of Ru films versus RuO_x films by CVD is dependent on both the temperature of deposition and the partial pressure of oxygen available at the surface of the growing film, where a clear delineation exists between the conditions necessary for the metal and the oxide.[46] Although it is perhaps not surprising for such a phase diagram to exist for CVD-grown materials, few examples of such reactivity occurring in an ALD process with a single precursor over a narrow temperature window exist.[35] This behavior, however, may be general for all metals for which the reduction potential from the oxide to the metallic form is positive relative to the standard hydrogen electrode.

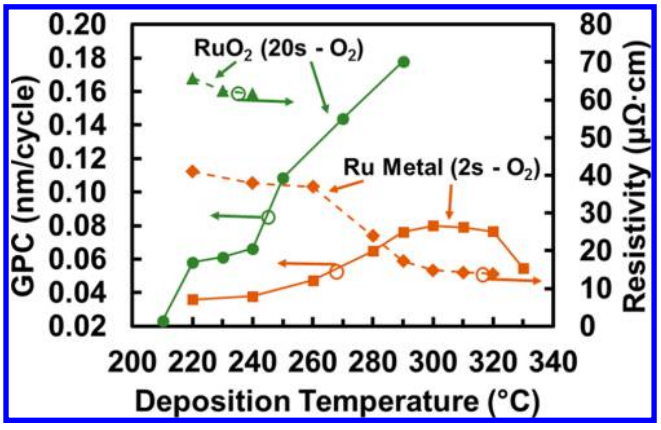

Figure 14. Comparison of GPC and resistivity vs temperature for Ru and RuO_2 thermal ALD processes. The 20 s O_2 pulses are shown as green circles (GPC) and green triangles (resistivity) and the 2 s O_2 pulses as orange squares (GPC) and orange diamonds (resistivity).

With respect to the O_2 pulse time, the RuO_2 GPC saturates (as shown in Figure 9b) whereas the Ru GPC does not (Figure 3b). This is consistent with an ALD system in which the O_2 dose is a key determinant, along with temperature as described above, for whether Ru or RuO_2 is obtained. As predicted by Kang et al.,[46] a large oxygen dose at lower temperatures provides RuO_2 films, whereas an oxygen-poor environment at higher temperatures results in low-resistivity Ru metal.

The growth rate and film properties for either process outside the ALD window also are informative. Again with respect to Figure 14, for Ru, the deposition rate decreases at temperatures below the ALD window. This decrease in deposition rate is accompanied by an increase in film resistivity, indicating formation of RuO_x. As the O_2 pulse is only 2 s long, the GPC of RuO_x is much lower than that for the 20 s O_2 pulse RuO_2 process. The deposition rate for RuO_2 increases above the ALD window. As oxygen becomes mobile above 250 °C in RuO_2, longer O_2 pulses lead to an increased concentration of subsurface oxygen that can escape the film and react at the surface, causing CVD-like growth during the Ru pulse. It can be surmised that because carbonyl ligands are well-known to be labile and can dissociate from metals under mild conditions, a probable mechanism for reaction would involve loss of CO and the formation of a metal−surface bond. The fact that DMBD is both chelating and π-backbonding would help otherwise stabilize this surface functionalization between Ru precursor and O_2 exposures. It is proposed that the DMBD ligand would be retained on the ruthenium metal center subsequent to chemisorption and should be liberated or consumed only upon the subsequent co-reactant pulse. Thus, it is the supply of the co-reactant (O_2) from the subsurface that allows additional reaction during the Ru pulse.

5. SUMMARY AND CONCLUSIONS

We have investigated the suitability of a zero-oxidation state precursor, η^4-2,3-dimethylbutadiene ruthenium tricarbonyl [$Ru(DMBD)(CO)_3$], with regard to both Ru and RuO_2 film growth. Ru films were successfully deposited with thermal

DOI: 10.1021/acs.chemmater.6b04251
Chem. Mater. 2017, 29, 1107−1115

ALD. Using 2 s pulses of O_2, a saturating growth rate of 0.067 nm/cycle with negligible nucleation delay is observed within an ALD temperature window of 290−320 °C. The Ru metal shows a strong hexagonal crystal structure with a low resistivity of approximately 14 $\mu\Omega$ cm at 320 °C and a fairly smooth surface roughness of ∼0.6 nm for 8 nm thick films.

Using 20 s long oxygen pulses and lower temperatures, RuO_2 films were deposited by both thermal and PEALD using O_2 or O_2 plasma. The temperature window for thermal ALD RuO_2 (220−240 °C) is slightly higher than that of PEALD RuO_2 (200−230 °C). Thermal RuO_2 exhibits a GPC higher than and a nucleation delay on SiO_2 substrates shorter than those of PEALD RuO_2, with 0.065 and 0.029 nm/cycle and 35 and 76 cycles, respectively. RuO_2 films grown by thermal ALD also show distinct rutile phase microstructure with a resistivity of ∼62 $\mu\Omega$ cm, a density close to bulk, and RMS roughness of 0.6 nm for 12 nm thick films. PEALD RuO_2 films exhibit less distinct crystallinity with much higher resistivity. The lower growth rate, longer nucleation delay, and higher resistivity are likely due to O_2 plasma etching of the growing RuO_2 film.

Overall, $Ru(DMBD)(CO)_3$ appears to be a promising precursor for thermal ALD of both Ru and RuO_2 thin films. Processes based on this precursor offer the advantages typical for ALD but also provide improvements over many of the known processes for these materials, including resistivity and nucleation behavior. In addition, the potential ability of the deposited morphology to be used as a template for rutile TiO_2 may facilitate fabrication of high-k MIM capacitors. Considering the emerging applications for Ru-containing thin film materials for various architectures anticipated in future ULSI device nodes, the work presented here is an important addition to the existing reported methods.

AUTHOR INFORMATION

Corresponding Author

*E-mail: jconley@eecs.oregonstate.edu.

ORCID

Dustin Z. Austin: 0000-0001-9580-4711

Notes

The authors declare no competing financial interest.

ACKNOWLEDGMENTS

The authors thank J. McGlone for AFM characterization, C. Tasker for equipment support, T. Mueller for performing XPS analysis, and ON Semiconductor and the Oregon Nanoscience and Microtechnologies Institute (ONAMI) for partial financial support. Part of this work was conducted at the Materials Synthesis and Characterization (MaSC) Center, a National Nanotechnology Coordinated Infrastructure (NNCI) Northwest Nanotechnology Infrastructure (NWNI) user facility at Oregon State University, which is supported in part by the National Science Foundation (Grant ECC-1542101) and Oregon State University.

REFERENCES

(1) Lane, M. W.; Murray, C. E.; McFeely, F. R.; Vereecken, P. M.; Rosenberg, R. Liner Materials for Direct Electrodeposition of Cu. *Appl. Phys. Lett.* **2003**, *83*, 2330.

(2) Han, J. H.; Han, S.; Lee, W.; Lee, S. W.; Kim, S. K.; Gatineau, J.; Dussarrat, C.; Hwang, C. S. Improvement in the Leakage Current Characteristic of Metal-Insulator-Metal Capacitor by Adopting RuO_2 Film as Bottom Electrode. *Appl. Phys. Lett.* **2011**, *99*, 022901.

(3) Hudec, B.; Hušeková, K.; Dobročka, E.; Aarik, J.; Rammula, R.; Kasikov, A.; Tarre, A.; Vincze, A.; Fröhlich, K. Atomic Layer Deposition Grown Metal-Insulator-Metal Capacitors with RuO_2 Electrodes and Al-Doped Rutile TiO_2 Dielectric Layer. *J. Vac. Sci. Technol., B: Nanotechnol. Microelectron.: Mater., Process., Meas., Phenom.* **2011**, *29*, 01AC09.

(4) Frohlich, K.; Hudec, B.; Tapajna, M.; Husekova, K.; Rosova, A.; Elias, P.; Aarik, J.; Rammula, R.; Kasikov, A.; Arroval, T.; Aarik, L.; Murakami, K.; Rommel, M.; Bauer, A. J. TiO_2-Based Metal-Insulator-Metal Structures for Future DRAM Storage Capacitors. *ECS Trans.* **2013**, *50*, 79−87.

(5) Ibidunni, A. O. The Oxidation and Resistance of Tantalum-Nitride Thin Films. *Oxid. Met.* **1993**, *40*, 5−20.

(6) Salaün, A.; Newcomb, S. B.; Povey, I. M.; Salaün, M.; Keeney, L.; O'Mahony, A.; Pemble, M. E. Nucleation and Chemical Transformation of RuO_2 Films Grown on (100) Si Substrates by Atomic Layer Deposition. *Chem. Vap. Deposition* **2011**, *17*, 114−122.

(7) Kim, W.-H.; Park, S.-J.; Kim, D.; Kim, H. Atomic Layer Deposition of Ruthenium and Ruthenium-Oxide Thin Films by Using a $Ru(EtCp)_2$ Precursor and Oxygen Gas. *J. Korean Phys. Soc.* **2009**, *55*, 32.

(8) Kwon, O.-K.; Kim, J.-H.; Park, H.-S.; Kang, S.-W. Atomic Layer Deposition of Ruthenium Thin Films for Copper Glue Layer. *J. Electrochem. Soc.* **2004**, *151*, G109.

(9) Kwon, S.-H.; Kwon, O.-K.; Kim, J.-H.; Jeong, S.-J.; Kim, S.-W.; Kang, S.-W. Improvement of the Morphological Stability by Stacking RuO_2 on Ru Thin Films with Atomic Layer Deposition. *J. Electrochem. Soc.* **2007**, *154*, H773.

(10) Kim, J.-H.; Kil, D.-S.; Yeom, S.-J.; Roh, J.-S.; Kwak, N.-J.; Kim, J.-W. Modified Atomic Layer Deposition of RuO_2 Thin Films for Capacitor Electrodes. *Appl. Phys. Lett.* **2007**, *91*, 052908.

(11) Kim, J. W.; Son, K. S.; Kim, B.; Kim, W.; Shim, J. H. Atomic Layer Deposition of Ruthenium in Various Precursors and Oxygen Doses. *ECS Trans.* **2013**, *50*, 165−171.

(12) Park, S.-J.; Kim, W.-H.; Lee, H.-B.-R.; Maeng, W. J.; Kim, H. Thermal and Plasma Enhanced Atomic Layer Deposition Ruthenium and Electrical Characterization as a Metal Electrode. *Microelectron. Eng.* **2008**, *85*, 39−44.

(13) Yim, S.-S.; Lee, D.-J.; Kim, K.-S.; Kim, S.-H.; Yoon, T.-S.; Kim, K.-B. Nucleation Kinetics of Ru on Silicon Oxide and Silicon Nitride Surfaces Deposited by Atomic Layer Deposition. *J. Appl. Phys.* **2008**, *103*, 113509.

(14) Aoyama, T.; Eguchi, K. Ruthenium Films Prepared by Liquid Source Chemical Vapor Deposition Using Bis-(Ethylcyclopentadienyl) Ruthenium. *Jpn. J. Appl. Phys.* **1999**, *38*, L1134.

(15) Matsui, Y.; Hiratani, M.; Nabatame, T.; Shimamoto, Y.; Kimura, S. Characteristics of Ruthenium Films Prepared by Chemical Vapor Deposition Using Bis(ethylcyclopentadienyl)ruthenium Precursor. *Electrochem. Solid-State Lett.* **2002**, *5*, C18.

(16) Aaltonen, T.; Alén, P.; Ritala, M.; Leskelä, M. Ruthenium Thin Films Grown by Atomic Layer Deposition. *Chem. Vap. Deposition* **2003**, *9*, 45−49.

(17) Aaltonen, T.; Ritala, M.; Arstila, K.; Keinonen, J.; Leskelä, M. Atomic Layer Deposition of Ruthenium Thin Films from $Ru(thd)_3$ and Oxygen. *Chem. Vap. Deposition* **2004**, *10*, 215−219.

(18) Park, S.-J.; Kim, W.-H.; Maeng, W. J.; Yang, Y. S.; Park, C. G.; Kim, H.; Lee, K.-N.; Jung, S.-W.; Seong, W. K. Effect Oxygen Exposure on the Quality of Atomic Layer Deposition of Ruthenium from Bis(cyclopentadienyl)ruthenium and Oxygen. *Thin Solid Films* **2008**, *516*, 7345−7349.

(19) Kukli, K.; Kemell, M.; Puukilainen, E.; Aarik, J.; Aidla, A.; Sajavaara, T.; Laitinen, M.; Tallarida, M.; Sundqvist, J.; Ritala, M.; Leskelä, M. Atomic Layer Deposition of Ruthenium Films from (Ethylcyclopentadienyl) (pyrrolyl)ruthenium and Oxygen. *J. Electrochem. Soc.* **2011**, *158*, D158.

(20) Knaut, M.; Junige, M.; Albert, M.; Bartha, J. W. In-Situ Real-Time Ellipsometric Investigations during the Atomic Layer Deposition of Ruthenium: A Process Development from [(Ethylcyclopentadienyl)

DOI: 10.1021/acs.chemmater.6b04251
Chem. Mater. 2017, 29, 1107−1115

(pyrrolyl)ruthenium] and Molecular Oxygen. *J. Vac. Sci. Technol., A* **2012**, *30*, 01A151.
(21) Kukli, K.; Aarik, J.; Aidla, A.; Jõgi, I.; Arroval, T.; Lu, J.; Sajavaara, T.; Laitinen, M.; Kiisler, A.-A.; Ritala, M.; Leskelä, M.; Peck, J.; Natwora, J.; Geary, J.; Spohn, R.; Meiere, S.; Thompson, D. M. Atomic Layer Deposition of Ru Films from bis(2,5-Dimethylpyrrolyl) ruthenium and Oxygen. *Thin Solid Films* **2012**, *520*, 2756−2763.
(22) Gregorczyk, K.; Henn-Lecordier, L.; Gatineau, J.; Dussarrat, C.; Rubloff, G. Atomic Layer Deposition of Ruthenium Using the Novel Precursor bis(2,6,6-Trimethyl-Cyclohexadienyl)ruthenium. *Chem. Mater.* **2011**, *23*, 2650−2656.
(23) Methaapanon, R.; Geyer, S. M.; Lee, H.-B.-R.; Bent, S. F. The Low Temperature Atomic Layer Deposition of Ruthenium and the Effect of Oxygen Exposure. *J. Mater. Chem.* **2012**, *22*, 25154.
(24) van der Straten, O.; Rossnagel, S. M.; Doyle, J. P.; Rodbell, K. P. Metal-Organic Atomic Layer Deposition of Metals for Applications in Interconnect Technology. *ECS Trans* **2005**, *1*, 51−56.
(25) Leick, N.; Verkuijlen, R. O. F.; Lamagna, L.; Langereis, E.; Rushworth, S.; Roozeboom, F.; van de Sanden, M. C. M.; Kessels, W. M. M. Atomic Layer Deposition of Ru from $CpRu(CO)_2Et$ Using O_2 Gas and O_2 Plasma. *J. Vac. Sci. Technol., A* **2011**, *29*, 021016.
(26) Park, S. K.; Kanjolia, R.; Anthis, J.; Odedra, R.; Boag, N.; Wielunski, L.; Chabal, Y. J. Atomic Layer Deposition of Ru/RuO_2 Thin Films Studied by In Situ Infrared Spectroscopy. *Chem. Mater.* **2010**, *22*, 4867−4878.
(27) Leick, N.; Agarwal, S.; Mackus, A. J. M.; Kessels, W. M. M. Dehydrogenation Reactions during Atomic Layer Deposition of Ru Using O_2. *Chem. Mater.* **2012**, *24*, 3696−3700.
(28) Jung, H. J.; Han, J. H.; Jung, E. A.; Park, B. K.; Hwang, J.-H.; Son, S. U.; Kim, C. G.; Chung, T.-M.; An, K.-S. Atomic Layer Deposition of Ruthenium and Ruthenium Oxide Thin Films from a Zero-Valent (1,5-Hexadiene)(1-Isopropyl-4-Methylbenzene)-ruthenium Complex and O_2. *Chem. Mater.* **2014**, *26*, 7083−7090.
(29) Choi, S.-H.; Cheon, T.; Kim, S.-H.; Kang, D.-H.; Park, G.-S.; Kim, S. Thermal Atomic Layer Deposition (ALD) of Ru Films for Cu Direct Plating. *J. Electrochem. Soc.* **2011**, *158*, D351.
(30) Eom, T.-K.; Sari, W.; Choi, K.-J.; Shin, W.-C.; Kim, J. H.; Lee, D.-J.; Kim, K.-B.; Sohn, H.; Kim, S.-H. Low Temperature Atomic Layer Deposition of Ruthenium Thin Films Using Isopropylmethyl-benzene-Cyclohexadiene-Ruthenium and O_2. *Electrochem. Solid-State Lett.* **2009**, *12*, D85.
(31) Yeo, S.; Choi, S.-H.; Park, J.-Y.; Kim, S.-H.; Cheon, T.; Lim, B.-Y.; Kim, S. Atomic Layer Deposition of Ruthenium (Ru) Thin Films Using Ethylbenzen-Cyclohexadiene Ru(0) as a Seed Layer for Copper Metallization. *Thin Solid Films* **2013**, *546*, 2−8.
(32) Hong, T. E.; Choi, S.-H.; Yeo, S.; Park, J.-Y.; Kim, S.-H.; Cheon, T.; Kim, H.; Kim, M.-K.; Kim, H. Atomic Layer Deposition of Ru Thin Films Using a Ru(0) Metallorganic Precursor and O_2. *ECS J. Solid State Sci. Technol.* **2013**, *2*, P47−P53.
(33) Yeo, S.; Park, J.-Y.; Lee, S.-J.; Lee, D.-J.; Seo, J. H.; Kim, S.-H. Ruthenium and Ruthenium Dioxide Thin Films Deposited by Atomic Layer Deposition Using a Novel Zero-Valent Metalorganic Precursor, (ethylbenzene)(1,3-butadiene)Ru(0), and Molecular Oxygen. *Microelectron. Eng.* **2015**, *137*, 16−22.
(34) Park, J.-Y.; Yeo, S.; Cheon, T.; Kim, S.-H.; Kim, M.-K.; Kim, H.; Hong, T. E.; Lee, D.-J. Growth of Highly Conformal Ruthenium-Oxide Thin Films with Enhanced Nucleation by Atomic Layer Deposition. *J. Alloys Compd.* **2014**, *610*, 529−539.
(35) Hämäläinen, J.; Ritala, M.; Leskelä, M. Atomic Layer Deposition of Noble Metals and Their Oxides. *Chem. Mater.* **2014**, *26*, 786−801.
(36) Song, Y. W.; Lee, J.; Lee, K.; Lee, Y.; Jang, H. K. Atomic Layer Deposition of Ru by Using a New Ru-Precursor. *ECS Trans.* **2006**, *2*, 1−11.
(37) Cheon, T.; Choi, S.-H.; Kim, S.-H.; Kang, D.-H. Atomic Layer Deposition of RuAlO Thin Films as a Diffusion Barrier for Seedless Cu Interconnects. *Electrochem. Solid-State Lett.* **2011**, *14*, D57.
(38) Basolo, F. Kinetics and mechanisms of CO substitution of metal carbonyls. *Polyhedron* **1990**, *9*, 1503−1535.
(39) Gambino, O.; Valle, M.; Aime, S.; Vaglio, G. A. Butadienic Derivatives and Metal Carbonyls II. Some Rearrangements of Butadienic Ligands in Reactions with Dodecacarbonyltriruthenium. *Inorg. Chim. Acta* **1974**, *8*, 71−75.
(40) Price, D. M. Vapor Pressure Determination by Thermogravimetry. *Thermochim. Acta* **2001**, *367*−*368*, 253−262.
(41) Cardarelli, F. *Materials Handbook: A Concise Desktop Reference*, 2nd ed.; Springer: London, 2008.
(42) Moulder, J. F.; Stickle, W. F.; Sobol, P. E.; Bomben, K. D. In *Handbook of X-ray photoelectron spectroscopy: a reference book of standard spectra for identification and interpretation of XPS data*; Chastain, J., Ed.; Perkin-Elmer Corp.: Eden Prairie, MN, 1992.
(43) Ritala, M.; Kukli, K.; Rahtu, A.; Raisanen, P. I.; Leskela, M.; Sajavaara, T.; Keinonen, J. Atomic Layer Deposition of Oxide Thin Films with Metal Alkoxides as Oxygen Sources. *Science* **2000**, *288* (5464), 319−321.
(44) Böttcher, A.; Niehus, H. Formation of Subsurface Oxygen at Ru(0001). *J. Chem. Phys.* **1999**, *110*, 3186.
(45) Aaltonen, T.; Rahtu, A.; Ritala, M.; Leskelä, M. Reaction Mechanism Studies on Atomic Layer Deposition of Ruthenium and Platinum. *Electrochem. Solid-State Lett.* **2003**, *6*, C130.
(46) Kang, S. Y.; Choi, K. H.; Lee, S. K.; Hwang, C. S.; Kim, H. J. Thermodynamic Calculations and Metallorganic Chemical Vapor Deposition of Ruthenium Thin Films Using Bis (Ethyl-π-Cyclopentadienyl) Ru for Memory Applications. *J. Electrochem. Soc.* **2000**, *147*, 1161−1167.
(47) Choi, J.; Choi, Y.; Hong, J.; Tian, H.; Roh, J.-S.; Kim, Y.; Chung, T.-M.; Oh, Y. W.; Kim, Y.; Kim, C. G.; No, K. Composition and Electrical Properties of Metallic Ru Thin Films Deposited Using $Ru(C_6H_6)(C_6H_8)$ Precursor. *Jpn. J. Appl. Phys.* **2002**, *41*, 6852−6856.
(48) Pan, W.; Desu, S. B. Reactive Ion Etching of RuO_2 Films: The Role of Additive Gases in O_2 Discharge. *Phys. Status Solidi A* **1997**, *161*, 201−215.

DOI: 10.1021/acs.chemmater.6b04251
Chem. Mater. 2017, 29, 1107−1115